Soft Matter

PAPER

View Article Online
View Journal | View Issue

Cite this: *Soft Matter*, 2022, **18**, 3087

All-atom simulations of bent liquid crystal dimers: the twist-bend nematic phase and insights into conformational chirality†

Gary Yu and Mark Richard Wilson *

The liquid crystal dimer 1,7-bis-4-(4′-cyanobiphenyl)heptane (CB7CB) is known to exhibit a nematic–nematic phase transition, with the lower temperature phase identified as the twist-bend nematic (N_{TB}) phase. Despite the achiral nature of the mesogen, the N_{TB} phase demonstrates emergent chirality through the spontaneous formation of a helical structure. We present extensive molecular dynamics simulations of CB7CB using an all-atom force field. The N_{TB} phase is observed in this model and, upon heating, shows phase transitions into the nematic (N) and isotropic phases. The simulated N_{TB} phase returns a pitch of 8.35 nm and a conical tilt angle of 29°. Analysis of the bend angle between the mesogenic units reveals an average angle of 127°, which is invariant to the simulated phase. We have calculated distributions of the chirality order parameter, χ, for the ensemble of conformers in the N_{TB} and N phases. These distributions elucidate that CB7CB is statistically achiral but can adopt chiral conformers with no preference for a specific handedness. Furthermore, there is no change in the extent of conformational chirality between the N_{TB} and N phases. Using single-molecule stochastic dynamics simulations in the gas phase, we study the dimer series CB*n*CB (where n = 6, 7, 8 or 9) and CBX$(CH_2)_5$YCB (where X/Y = CH_2, O or S) in terms of the bend angle and conformational chirality. We confirm that the bent molecular shape determines the ability of a dimer to exhibit the N_{TB} phase rather than its potential to assume chiral conformers; as $|\chi|_{max}$ increases with the spacer length, but the even-membered dimers have a linear shape in contrast to the bent nature of dimers with spacers of odd parity. For CBX$(CH_2)_5$YCB, it is found that $|\chi|_{max}$ increases as the bend angle of the dimer decreases, while the flexibility of the dimers remains unchanged through the series.

Received 3rd March 2022,
Accepted 24th March 2022

DOI: 10.1039/d2sm00291d

rsc.li/soft-matter-journal

1 Introduction

The simplest liquid crystal mesophase is the uniaxial nematic (N) phase, which is characterised by the orientational alignment of the molecules in a preferred direction but with low positional ordering. The introduction of chirality, either by a chiral centre within the mesogen or the addition of a chiral dopant into a host N phase, results in the formation of the chiral nematic (N*) phase which features a helical structure. Independently, Meyer[1] and Dozov[2] predicted that liquid crystal phases with local chirality could be formed by bent achiral mesogens which was, later, supported by Memmer[3] in computer simulations. Dozov proposed that a pure uniform bend in space, arising from the packing of bent molecules, is forbidden and, thus, twist or splay deformations of the local director must accompany the spontaneous bend. In the twist-bend nematic (N_{TB}) phase, a heliconical structure is formed in which the director is tilted with respect to the helical axis, where there are equal numbers of degenerate domains of opposite handedness.

The N_{TB} phase was first discovered for 1,7-bis-4-(4′-cyanobiphenyl)heptane, CB7CB, which consists of two mesogenic units connected by a flexible spacer.[4–7] The requisite bent molecular shape is exhibited in dimers with a hydrocarbon spacer of odd parity. Other dimeric mesogens,[8–17] bent-core species,[18,19] and supramolecular hydrogen-bonded systems[20–23] have been reported to manifest the N_{TB} phase. Despite the significant number of materials investigated, a general structure–property relationship for the N_{TB} phase remains elusive; although, it is found that a spatially uniform curvature of the molecule is necessary to form the N_{TB} phase regardless of the underlying chemical groups.[24,25] The addition of an intrinsic chiral centre into a bent dimer resolves the globally achiral N_{TB} into its chiral counterpart, the N_{TB}* phase, which only contains domains according to the handedness of the chiral centre.[26] By extending the length of the terminal alkyl chains,

Department of Chemistry, Durham University, Lower Mountjoy, Stockton Road, Durham, UK. E-mail: mark.wilson@durham.ac.uk

† Electronic Supplementary Information (ESI) available: Simulation input files and snapshot coordinates for the N_{TB}, nematic and isotropic phases. See DOI: 10.1039/d2sm00291d

achiral dimers can exhibit a heliconical smectic (SmC_{TB}) phase.[27–29] Possible applications utilising the N_{TB} phase such as optical devices,[30–33] gels,[34] photoswitchable adhesives,[35] and photoalignment technology[36] have been reported.

Molecular simulation is an effective tool in the study of liquid crystals.[37–39] In recent years, improvements in the accuracy of force fields and increase in available computational power has greatly benefited the modelling of these systems.[40] All-atom simulations have facilitated the contribution of numerous insights into liquid crystals including: structural, thermodynamic and phase-related properties of nematogens within mesophases and across the phase transitions;[41] optimisation of force fields to improve representation of phase transitions and physical properties;[42] calculation of molecular chirality and helical twisting powers;[43–48] simulation of a biaxial nematic phase;[49] predictions of the dark conglomerate phase formed by a bent-core mesogen;[50] and investigations of the emergent chirality in achiral bent-core molecules.[51–55] An early model for a liquid crystal dimer represented the rigid mesogenic segments with anisotropic Gay–Berne units which were connected by a flexible Lennard-Jones chain.[56] Simulations using this model demonstrated the spontaneous growth of smectic phases from the isotropic liquid. A similar model, at the same resolution, displays a N_x phase which was assigned as the polar-twisted N phase.[57] Further coarse-grained models, such as a crescent-shaped model of connected hard spheres[58] or curved spherocylinders,[59–61] successfully exhibit the N_{TB} phase. At the fully atomistic level, conformational probability distributions for CB7CB show a broad peak centred at approximately 120° for the molecular bend angle with a minor peak at about 30° corresponding to hairpin conformers.[4,16] Atomistic simulations have also captured the N_{TB} phase and are in good agreement with experimental findings.[6]

In this paper, we present extensive all-atom molecular dynamics (AA MD) simulations of the bent liquid crystal dimer CB7CB. We observe the formation of the N_{TB} phase, characterise its properties, and explore the CB7CB phase diagram as a function of temperature. The simulations provide a full description of the orientational order of molecules in the N and N_{TB} phases and a detailed examination of the structure of CB7CB molecules in these phases. We calculate distributions of the bend angle and chirality order parameter for molecules in the N and N_{TB} phases. Using single-molecule simulations in the gas phase, we expand the scope of the investigation to the dimer series CB*n*CB (where n = 6, 7, 8 or 9) and CBX$(CH_2)_5$YCB (where X/Y = CH_2, O or S). The effect of the spacer length and heteroatom linkages are discussed in terms of the conformational distributions of the bend angle and their molecular chirality.

2 Computational methods

2.1 Force field

The General AMBER Force Field (GAFF) was utilised for atomistic simulations.[62] The Antechamber package from AmberTools18[63] was employed to generate Lennard-Jones potentials and atomic charges for the force field, with the latter employing the AM1-BCC method.[64] The output GAFF topologies were converted into the necessary input files for GROMACS by the ACPYPE script.[65]

2.2 Simulation details

A bulk system was set up by randomly inserting 512 molecules of CB7CB, which were oriented with the molecular long axes aligned with the z-axis, into a box with dimensions of 8 nm × 8 nm × 16 nm. Initially, an additional improper dihedral potential (with an equilibrium angle of 180° and force constant of 25 kJ mol^{-1}) was applied across each molecule, between the terminal nitrogen atoms and the linking carbon of the mesogenic units with the alkyl spacer and the corresponding atoms on the other cyanobiphenyl segment, to enforce an all-*trans* configuration of the heptane chain.

All MD simulations were carried out using the GROMACS 2021.1 molecular dynamics simulation package.[66] A cutoff of 1.2 nm was used for all short-range interactions and long-range electrostatics were treated with the Particle Mesh Ewald (PME) method.[67] After a steepest-descent minimisation, a 100 ps pre-equilibration run in the *NVT* ensemble was carried out using the Berendsen thermostat followed by a 100 ps pre-equilibration in the *NPT* ensemble with the addition of the Berendsen barostat.[68] Simulations were performed using semi-isotropic pressure coupling which allows for the x/y and z dimensions of the system to vary independently. Time constants of 1 ps and 5 ps were used for the thermostat and barostat, respectively. The system was compressed with a pressure of 100 bar for 1 ns, before an equilibration run of 500 ps was carried out using the Nosé–Hoover thermostat[69,70] to maintain a constant temperature of 370 K, and the Parrinello–Rahman barostat[71] to keep the pressure constant at 1 bar. A leap-frog algorithm was employed with a time step of 1 fs for equilibration with an increase to 2 fs for production simulations, where constraints were implemented using the LINCS method.[72] At this point, the system exhibited a nematic phase which acted as an ideal starting configuration. A final equilibration of 1 ns was executed without the additional biasing potential to allow for equilibration of the molecular conformations and for the heliconical structure to start developing. Finally, a production simulation of 1 μs was performed. Equilibration was ensured by monitoring average values for thermodynamic and structural quantities, and checking that they were stabilised. MD simulations were carried out on the new N8 CIR supercomputer Bede, housed at Durham University, using one NVIDIA V100 GPU; achieving a performance of 180 ns day^{-1} on a ~30 000 atom system.

The concluding system at 370 K was used as the starting configuration for a heating/cooling sequence. Simulations were performed at 10 K intervals for 200 ns each in the temperature range of 350–470 K.

For the chirality order parameter calculations, the sampling of conformers was conducted *via* single-molecule simulations in the gas phase using a stochastic dynamics (SD) integrator at

a temperature of 370 K with a standard friction constant of 0.5 ps^{-1}. Each molecule was equilibrated for 1 ns before a 500 ns production run to obtain data with snapshots being collected in 1 ps intervals. For single-molecule MD simulations calculations there are no collisions with neighbouring molecules to exchange energy and aid molecules to traverse high conformational energy barriers. Consequently, SD provides improved conformational sampling for single molecules in comparison to standard MD thermostats.

All simulation snapshots were visualised in VMD, version 1.9.3.[73]

2.3 Orientational order parameter

The orientational order parameter, S_2, can be determined from diagonalisation of the order tensor

$$Q_{\alpha\beta} = \frac{1}{N}\sum_{i=1}^{N}\frac{1}{2}\left(3u_{i\alpha}u_{i\beta} - \delta_{\alpha\beta}\right), \quad (1)$$

where N is the number of molecules and $\delta_{\alpha\beta}$ is the Kronecker delta. The largest eigenvalue provides the value of S_2 and its associated eigenvector is the director, $\hat{\boldsymbol{n}}$, of the system. The unit vector, $\hat{\boldsymbol{u}}_i$, of the molecular long axis for a molecule i can be defined by the eigenvector corresponding to the lowest eigenvalue found by diagonalising the moment of inertia tensor for a molecule

$$I_{\alpha\beta} = \sum_i m_i\left(\boldsymbol{s}_i^2\delta_{\alpha\beta} - s_{i\alpha}s_{i\beta}\right), \quad (2)$$

where m_i is the mass of atom i, $\boldsymbol{s}_i$ is the vector between an atom i and the molecular centre of mass and α, β is the Cartesian axis. In this work, the molecular long axis, $\hat{\boldsymbol{u}}_i$, will henceforth be referred to as $\hat{\boldsymbol{a}}$ for CB7CB.

2.4 Chirality order parameter

Ferrarini *et al.* developed a surface chirality model to determine a chirality order parameter, χ, based on a molecular isosurface which describes the coupling between the surface chirality and orientational order of the molecule.[74–77] The value of χ is positive for right-handed conformers and negative for left-handed ones. Here, molecular isosurfaces were generated using the Simple Invariant Molecular Surface (SIMS) method developed by Vorobjev and Hermans.[78] This utilised a rolling sphere algorithm where a spherical probe with a diameter of 5 Å produced a corresponding van der Waals surface of a molecule with a point resolution of 10 dots per $Å^2$. Three tensors are obtained from the isosurface for the calculation of χ: the surface tensor ($\boldsymbol{T}$), the helicity tensor ($\boldsymbol{Q}$) and the ordering matrix ($\boldsymbol{S}$). Numerical integration of the normal vectors over the surface points yields $\boldsymbol{T}$, whereas integration over the molecular surface produces $\boldsymbol{Q}$. The ordering matrix, $\boldsymbol{S}$, is calculated by integration of an orientational distribution function involving an orienting potential describing the orientation of the solute molecule within a liquid crystal phase.[46] Finally, the chirality order parameter is calculated from

$$\chi = -\left(\frac{2}{3}\right)^{\frac{1}{2}}\left(Q_{xx}S_{xx} + Q_{yy}S_{yy} + Q_{zz}S_{zz}\right) \quad (3)$$

where S_{ii} are the diagonal elements of $\boldsymbol{S}$ and Q_{ii} are the diagonal elements of $\boldsymbol{Q}$. Both these components are expressed in the principal axis system of $\boldsymbol{T}$ which defines the molecular principal axes (T_{xx}, T_{yy} and T_{zz}) when diagonalised.

3 Results and discussion

3.1 Phase behaviour

The system of 512 molecules of CB7CB at 370 K exhibited a heliconical structure that was stable for hundreds of nanoseconds. A snapshot of this simulated phase is shown in Fig. 2(a) in which molecules are coloured in blue, purple or red according to their azimuth angle (ϕ) in the range $-180^\circ \leq \phi < -60^\circ$, $-60^\circ \leq \phi < 60^\circ$ and $60^\circ \leq \phi \leq 180^\circ$, respectively. The angle ϕ was calculated for the unit vector $\hat{\boldsymbol{a}}$ which corresponds to the molecular long axis of the molecule. A second unit vector $\hat{\boldsymbol{b}}$ can be defined as the unit vector which bisects the two vectors between a terminal nitrogen atom and the centre of mass (COM) of the molecule. A schematic for these unit vectors is shown in Fig. 1. From visual inspection, a helical structure is found where the molecules are tilted with respect to the helical axis which largely coincides with the z axis of the box. It is noted that the helix found here is left-handed and that, experimentally, there are equal domains of opposite handedness.

The defined unit vectors were utilised in the analysis of the system. An orientational correlation function, S_{bb}, can be calculated as a function of intermolecular distance along the helical axis, $r_\parallel$, by[79]

$$S_{bb}(r_\parallel) = \sum_i^N\sum_{j\neq i}^N c_{ij}\left(\hat{b}_i\cdot\hat{b}_j\right), \quad (4)$$

where

$$c_{ij} = \delta\left(|z_{ij}| - r_\parallel\right)\Big/\sum_i^N\sum_{j\neq i}^N\delta\left(|z_{ij}| - r_\parallel\right). \quad (5)$$

$S_{\mathrm{bb}}(r_\parallel)$ describes the polar correlations through the system (and is presented in Fig. 3(a)), z_{ij} is the distance with respect to the z components for the COMs of molecules i and j, and N is the number of molecules. The results show that $\hat{b}$ precesses about the helical axis through the system as expected in the $\mathrm{N_{TB}}$ phase. This behaviour has been found for simulated phases previously.[57,58] From this plot (shown in Fig. 3 for the final

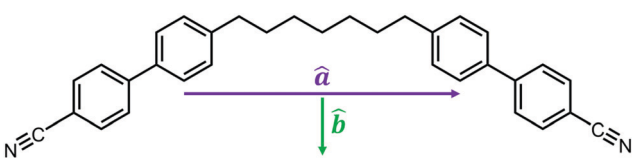

Fig. 1 Molecular structure of CB7CB, with a schematic for the unit vectors $\hat{\boldsymbol{a}}$ and $\hat{\boldsymbol{b}}$.

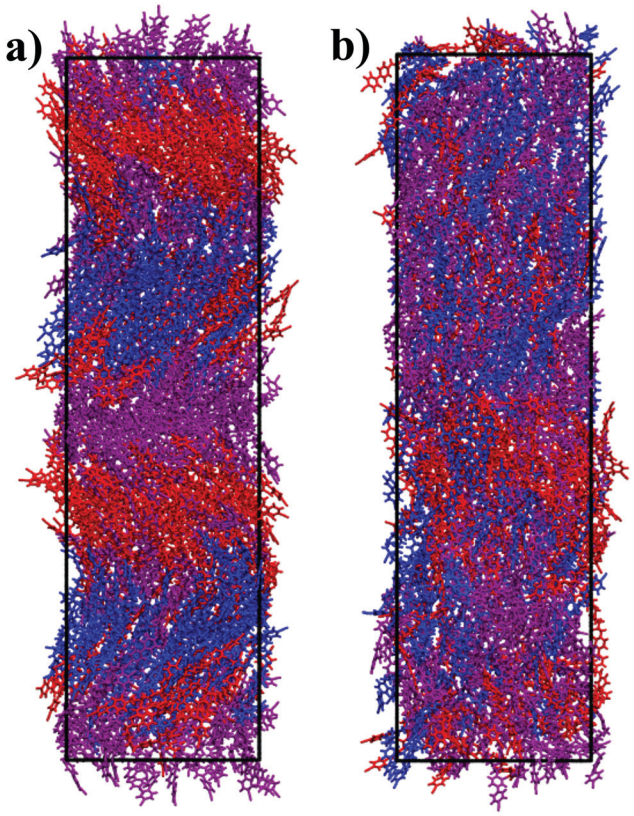

Fig. 2 Simulation snapshots of a 512 molecule system of CB7CB showing the (a) N_{TB} phase at 370 K and the (b) N phase at 440 K with orientational colouring (blue: $-180^\circ \leq \phi < -60^\circ$; purple: $-60^\circ \leq \phi < 60^\circ$; and red: $60^\circ \leq \phi < 180^\circ$).

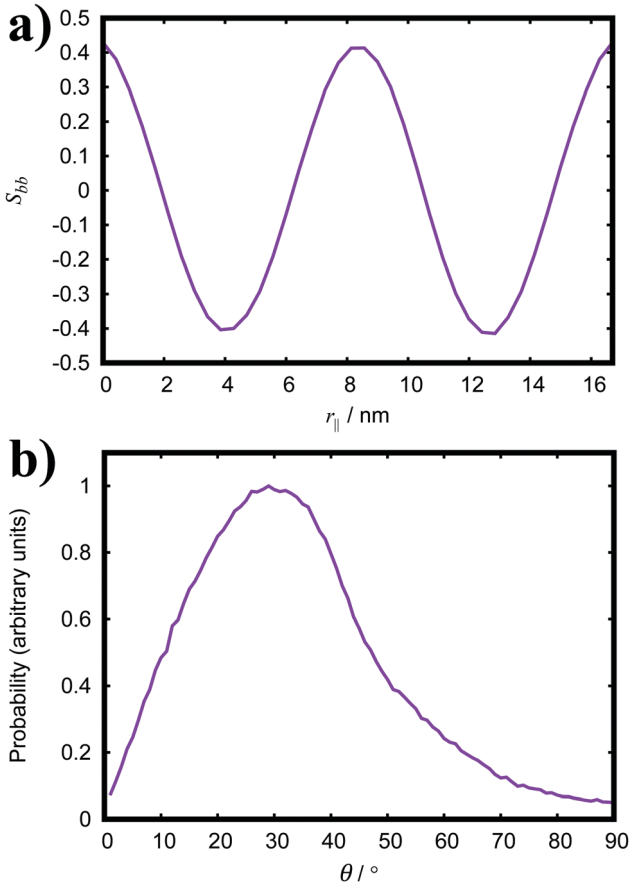

Fig. 3 (a) Orientational correlation (S_{bb}) as a function of the helical axis, $r_\parallel$, and the (b) distribution for the conical tilt angle, θ, for the N_{TB} phase at 370 K. For (a) the error bars are of the order of the line thickness (~0.01).

configuration at 370 K), it can be seen that minima/maxima occur at distances $(n + 1/2)p$, where n is 0, 1/2 and 1, and the pitch, p, is estimated to be 8.35 ± 0.2 nm. Our measured pitch is in good agreement with those found experimentally in the N_{TB} phase for CB7CB of ~8 nm.[6,7]

The conical tilt angle, θ, is defined as the angle between the unit vector $\hat{\boldsymbol{a}}$ and the helical axis. Noting that $\theta(z) = \pm|k|z = \pm 2\pi z/p$. A histogram of θ values observed in the system is shown in Fig. 3(b), which confirms that the molecules in the simulated phase are tilted with the average conical tilt angle measured to be 29°. Our simulation result is slightly higher than the ~25° reported experimentally.[6,80,81]

The simulated system at 370 K, which has been characterised as the N_{TB} phase, was cooled/heated in order to produced a full phase diagram for the AA model. Simulations were performed in the temperature range of 350–470 K and the average orientational order parameter, $\langle S_2 \rangle$, was determined for unit vectors $\hat{\boldsymbol{a}}$ and $\hat{\boldsymbol{b}}$. The results are presented in Fig. 4 in which the stability range of the N_{TB}, N and isotropic (I) phases are indicated. Here, we define the N_{TB}–N phase transition as the temperature at which helical ordering is lost ($\langle S_2 \rangle_b \approx 0$) and the I phase is identified when, additionally, $\langle S_2 \rangle_a \approx 0.1$. It is noted that, *via* visual inspection, the system at 430 K appears nematic but does not satisfy the aforementioned criteria for the

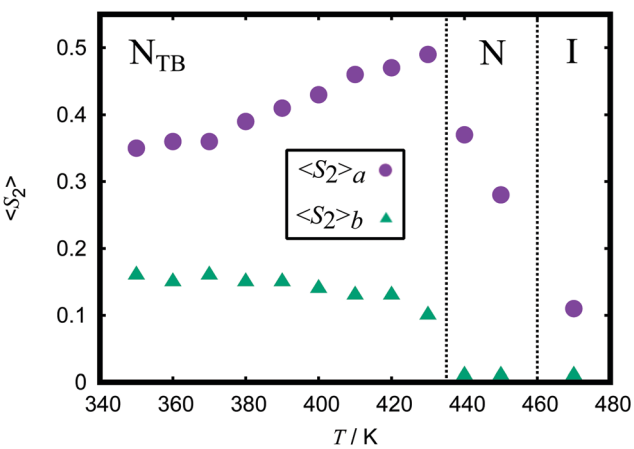

Fig. 4 Average orientational order parameter, $\langle S_2 \rangle$, for unit vectors $\hat{\boldsymbol{a}}$ and $\hat{\boldsymbol{b}}$ as a function of temperature.

N phase. A simulation snapshot of the N phase for CB7CB at 440 K is shown in Fig. 2(b). For $\langle S_2 \rangle_b$, this value diminishes slightly as the system is heated which is expected as the helix unwinds upon its approach into the N phase.[80] For $\langle S_2 \rangle_a$, the

nematic-like ordering increases with temperature throughout the N_{TB} phase until the phase transition into the N phase. This trend is observed in X-ray and polarised Raman scattering experiments and our measured values for $\langle S_2 \rangle_a$ of $\sim$0.35 in the N_{TB} phase (and subsequent values in the N phase) compare favourably.[81,82] However, the phase transitions in the AA model, $T_{N_{TB}-N}$ = 435 K and T_{N-I} = 460 K, occur at temperatures higher than reported[7] (experimentally, $T_{N_{TB}-N}$ = 376 K and T_{N-I} = 389 K). We suggest that the force field for CB7CB produces molecules that are slightly too stiff, thus mesogens are slightly elongated favouring orientational ordering and require slightly more energy to induce conformational changes. Both effects tend to increase transition temperatures. The force field would require further optimisation of the interatomic interaction parameters to reproduce the correct phase transitions. This has been demonstrated for GAFF in studies of liquid crystals systems, where the representation of structural and phase properties have been improved.[42,50,53,83]

3.2 Conformational distributions and molecular chirality

The following section focuses on the conformational properties of bent dimer mesogens and their ability to exhibit chiral conformations. The bend angle of the mesogen can be defined as the angle between the unit vectors representing the para axes of the cyanobiphenyl units (*i.e.* the vector calculated between the nitrogen atom and the carbon atom connecting the cyanobiphenyl unit to the spacer). Based on the simulations performed in the previous section, Fig. 5 shows histograms of this bend angle for CB7CB in the N and N_{TB} phases. In both phases, the average bend angle is found to be 127°. This is somewhat higher than the value of $\sim$120° determined by Monte Carlo sampling in previous single-molecule studies[4,16] but in line with a bulk phase MD simulation[6] value of 133°. It is found that the bend angle distribution does not change significantly between molecules in the N and N_{TB} phases but the broadness of the peak in the N phase increases, as expected for the higher temperature. The histograms also show a minor peak at 20° corresponding to hairpin conformers. NMR experiments suggest that the conformational distribution for CB7CB does not change significantly between the N and N_{TB} phases and that the chirality of the N_{TB} phase is a consequence of the bent molecular shape.[84]

Distributions of the chirality order parameter, χ, were calculated for CB7CB for molecules in the N and N_{TB} phases, and for a single molecule in the gas phase. These are presented in Fig. 6(a). All three plots demonstrate that CB7CB is statistically achiral (with the peaks centred at χ = 0) but can adopt chiral conformers with equal probability of left- or right-handedness (as the peaks are symmetric). This behaviour has been reported previously in single-molecule simulations of the P*n*OPIMB series of bent-core mesogens.[52,53] The aforementioned calculations found, for similar model parameters, values of $|\chi|_{max}$ to be $\sim$800 and greater whereas, in this work, we have estimated $|\chi|_{max}$ to be $\sim$200 for CB7CB. The much higher $|\chi|_{max}$ for the bent-core molecules, compared to CB7CB, may account for why P8OPIMB can form the highly twisted B4 phase which consists of helical nanofilaments.[85] The ability of achiral bent-core mesogens[51,52] and CB7CB[86,87] to decrease the pitch of a N* phase is hypothesised to be a result of the presence of chiral conformers with high helical twisting powers.[52,53] Interestingly, the distributions of χ are unchanged between the N and N_{TB} phases, which indicates that there is no change in the molecular chirality of the conformations even as the phase gains chirality. This is in line with analogous findings for the conformational distributions.[84] The analysis of the molecular chirality for a single molecule in the gas phase produces a distribution that is very similar to that from the condensed

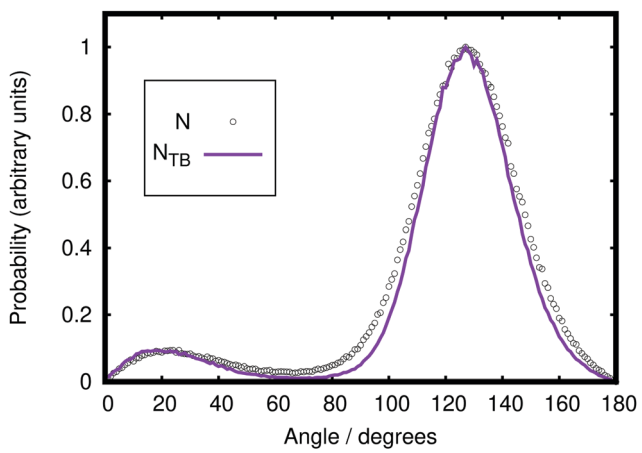

Fig. 5 Distribution functions for the bend angle between the mesogenic units in the N and N_{TB} phases at 440 K and 370 K, respectively.

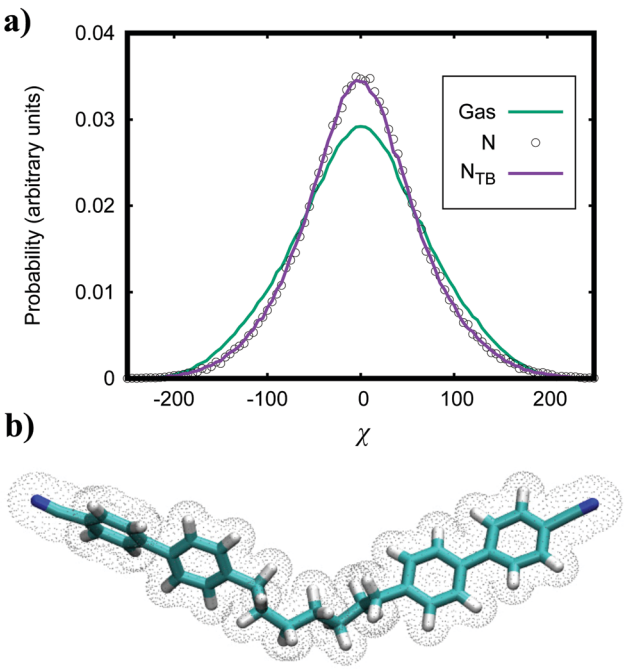

Fig. 6 (a) Distribution functions of the chirality order parameter, χ, for a single molecule in the gas phase and for molecules in the N (440 K) and N_{TB} (370 K) phases. (b) A conformer of CB7CB with its molecular isosurface shown.

phases with the exception that the peak is broader. This is expected as there is greater freedom for the molecule to sample a wider range of conformers in the gas phase.

From Fig. 6(a), it can be seen that sampling of conformers *via* a single-molecule simulation provides a good approximation for the distributions of χ obtained from simulations of the liquid crystal phases. This approach is relatively facile as the full calculations, from the automated generation of the force field/input files to the acquisition of the χ distribution, takes $\sim$20 hours and does not require a liquid crystal phase to be equilibrated. Thus, we can expand the scope of our investigation to the series of bent dimers CB*n*CB (where n = 6, 7, 8 or 9) and CBX$(CH_2)_5$YCB (where X/Y = CH_2, O or S). The first series of mesogens allows for the odd–even effect and the effect of the spacer length on the conformations/chirality of the molecule to be studied. The second series consists of bent dimers all with 7 heavy atoms in the spacer and considers the effect of heteroatoms in the linking chain.

The odd–even effect of the spacer on typical liquid crystalline phase behaviour is well-documented, and the N_{TB} phase is only found for odd-membered mesogenic dimers.[88–90] It is found that, in the all-*trans* configuration, dimers with an odd spacer will exhibit a bent molecular shape whereas an even spacer will result in a more linear shape. Moreover, the sensitivity of $T_{N_{TB}–N}$ to the bend angle has been demonstrated by a generalised Maier–Saupe theory.[91] Bend angle distributions for the CB*n*CB series are shown in Fig. 7(a). We obtain mean bend angles of 165°, 110°, 172° and 99° for n = 6, 7, 8 and 9, respectively at 370 K. Previously reported values include 166° for CB6CB,[6] 111–120° for CB7CB,[4,16,92] and 102° for CB9CB.[93] Overall, our measured values are in good agreement with previous work and the correct trend is observed. Notably, the bend angle for CB7CB in the gas phase is lower than in the N and N_{TB} phases, which suggests that the effect of a nematic environment on the conformational distribution is significant. This indicates that single-molecule calculations, regardless of the level of theory, are not truly representative of the actual behaviour within a mesophase. This is expected as the constraints arising from the packing of molecules in the N phase will affect the conformers adopted by the mesogens as well as promote a more linear shape of the molecules.[94,95] For the even-membered dimers, the dominant conformers are those with linear configurations, but there is the presence of a significant number of bent conformers with bend angles of around 85° and 130° for CB6CB and CB8CB, respectively. These bent conformers are likely to be suppressed strongly in the N phase.

The χ distributions for the CB*n*CB series are presented in Fig. 7(b) and all show that the mesogens are statistically achiral but can adopt chiral conformers of opposite handedness with equal probability. The histograms for CB6CB and CB8CB are noticeably narrower than those for the dimers with odd spacers. This demonstrates that the more linear shape of the even-membered dimers results in a lower tendency to exhibit instantaneous conformations with high helical twisting powers. For n = 6, 7 and 8, $|\chi|_{max} \approx 200$ but is $\sim$250 for

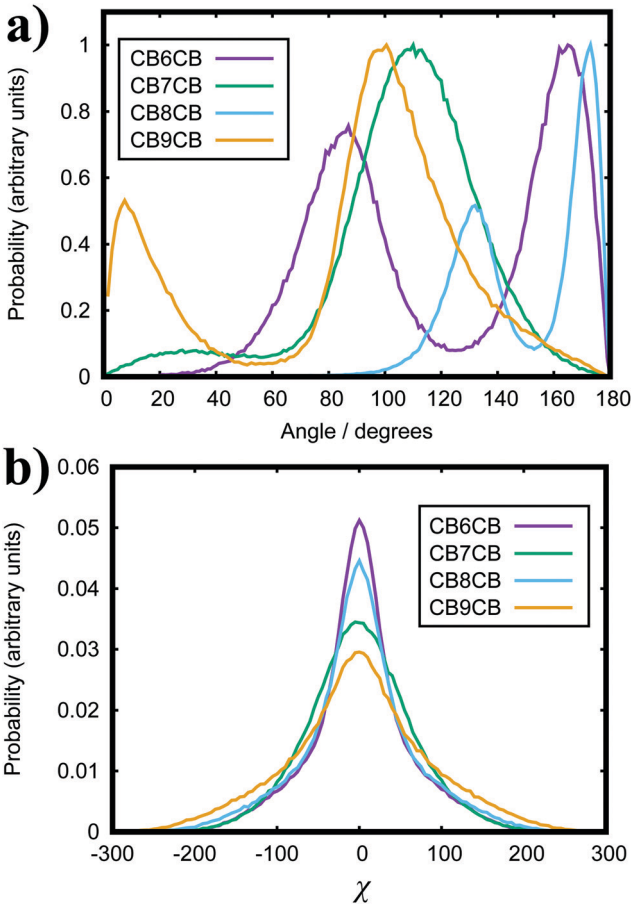

Fig. 7 Distribution functions of the (a) bend angle and (b) chirality order parameter, χ, for CB*n*CB where n = 6, 7, 8 or 9.

CB9CB. It seems that there is a slight increase in $|\chi|_{max}$ as the length of the spacer increases regardless of the odd/even parity of the chain. This suggests strongly that the ability to form the N_{TB} phase for dimers with a spacer of odd parity, or only exhibit the N phase for dimers with a spacer of even parity, is dependent on the molecular shape of the mesogen and not its potential to assume chiral conformers.[96]

In the CBX$(CH_2)_5$YCB series (where X/Y = CH_2, O or S), the N_{TB} phase is observed for all molecules.[16,92,97–99] While it is generally considered that CBO *n*OCB homologues mainly form the N phase, the presence of a N_{TB} phase is indicated for CBO5OCB by changes in the optical texture upon supercooling.[100,101] Here, we measure peaks in the bend angle distribution (see Fig. 8(a)) of 116° for CB6OCB, 110° for CB6SCB, 120° for CBO5OCB, 100° for CBS5SCB and 112° for CBS5OCB. Conformational sampling provides a reported value of $\sim$120° for CB6OCB[16] and optimised geometries of dimers, with all-*trans* configurations of the spacer,[92] give bend angles of 143° for CBO5OCB, 94° for CBS5SCB and 119° for CBS5OCB. Our results compare favourably with the exception of CBO5OCB.[92] It is noted that this literature value was obtained from a single conformer, albeit the minimum energy geometry, which does not consider the flexibility of the molecule.

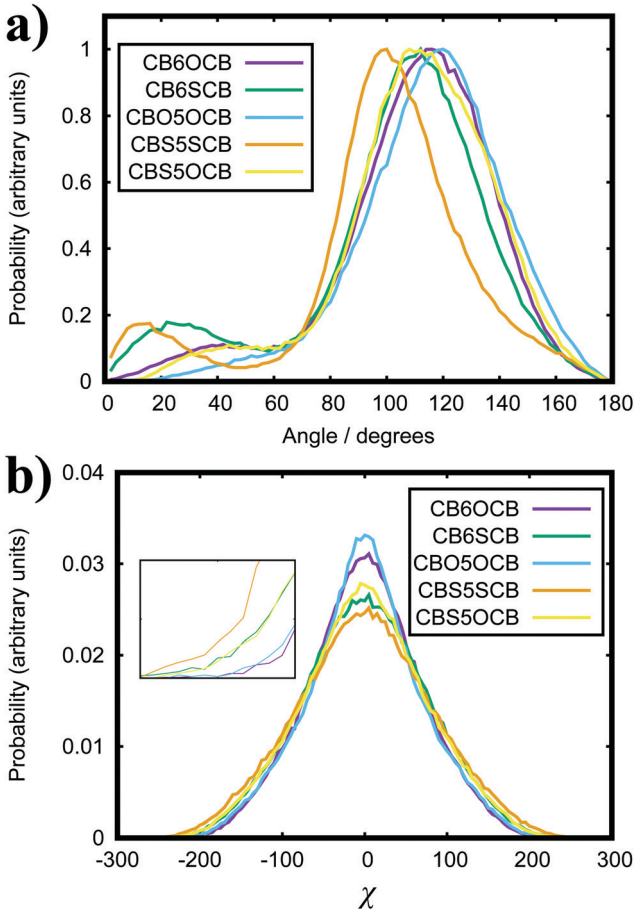

Fig. 8 Distribution functions of the (a) bend angle and (b) chirality order parameter, χ, for CBX$(CH_2)_5$YCB where X/Y = CH_2, O or S. The inset shows a focused view of the plot near $|\chi|_{max}$.

Since the CBX$(CH_2)_5$YCB (where X/Y = CH_2, O or S) series all have spacer lengths of 7 heavy atoms, any differences will mostly arise from the bond angle and flexibility afforded by the heteroatom linkage. The χ distributions are presented in Fig. 8(b). Here, we observe that the distributions get broader and $|\chi|_{max}$ increases for bent dimers in the order CBO5OCB, CB6OCB, CBS5OCB, CB6SCB to CBS5SCB. This is also the sequence of dimers going from the highest to lowest average bend angle measured here. Thus, we obtain the trend that a lower bend angle results in a higher degree of conformational chirality. Experimentally, the effect of the bend angle on $T_{N_{TB}-N}$ is unclear. The sulfur-linked dimers unexpectedly exhibit a lower $T_{N_{TB}-N}$ than the methylene versions despite having a smaller bend angle.[92,100] As $|\chi|_{max}$ is commensurate with the bend angle, we similarly do not observe any correlation between the presence of high χ conformers and the stability of the N_{TB} phase or transition temperatures. The full width at half maximum of the main peaks in Fig. 8a (which is a measure of the flexibility) is $\sim 50^\circ$ for CB7CB and all the CBX$(CH_2)_5$YCB dimers, and so it cannot be said that there is a strong link between the flexibility (*i.e.* polydispersity of bend angles) and $T_{N_{TB}-N}$.

4 Conclusions

In conclusion, we have presented extensive AA MD results for the bent liquid crystal dimer CB7CB. The simulations show a N_{TB} phase, which has a pitch of 8.35 nm and a conical tilt angle of 29°. Upon heating, phase transitions into the N and I phases are observed but $T_{N_{TB}-N}$ and T_{N-I} are overestimated. We suggest that improvements to the force field could be made, according to previously reported methodologies,[42,50,53,83] to better represent the transition temperatures. Analysis of the bend angle between the cyanobiphenyl units for CB7CB produces an average value of 127°, which is invariant between the N_{TB} and N phases. Distributions of the chirality order parameter, χ, demonstrate that CB7CB is statistically achiral but can adopt chiral conformers of opposite handedness with equal probability, and that the degree of molecular chirality is unchanged between the N_{TB} and N phases.

Using single-molecule simulations in the gas phase, distributions of the bend angle and χ are determined for the series of dimers CB*n*CB (where n = 6, 7, 8 or 9) and CBX$(CH_2)_5$YCB (where X/Y = CH_2, O or S). We obtain bend angles in good agreement with previously reported values with a simple and fast process. For CB*n*CB, we confirm that the ability to exhibit the N_{TB} phase is dependent on a bent molecular shape and not from the potential of the dimer to assume chiral conformers. For CBX$(CH_2)_5$YCB, we report that a decrease in the bend angle increases $|\chi|_{max}$. This corresponds to an increase in the extent of instantaneous chiral conformations for dimers with higher bent molecular curvature, despite the flexibility being similar.

The workflow presented here is easily automated, could be coupled with optimised parameters for the force field, and provides a route for high-throughput analysis of various properties of liquid crystal mesogens.

Finally, we note that all-atom simulations of the type described here provide unique insights into how molecules are arranged at the molecular level in complex mesophases, such as the N_{TB}. Future atomistic studies of other materials are likely to provide valuable insights into how molecular structure is related to the range of stability of N_{TB} phases. The influence of subtle changes in molecular shape, interactions and flexibility is very difficult to capture within a simple coarse-grained model. However, we are currently developing bottom-up coarse-grained approaches to multiscale modelling. These approaches use conformational and through-space interactions from an underlying atomistic reference to provide new coarse-grained molecular models that incorporate flexibility and aim to capture the influence of subtle changes in molecular structure on phase behaviour.[102,103] This work will facilitate the study of these fascinating liquid crystal phases on larger length and time scales.

Conflicts of interest

There are no conflicts to declare.

Acknowledgements

This research was supported by Durham University and EPSRC (EP/R513039/1). This work made use of the facilities, Bede, of the N8 Centre of Excellence in Computationally Intensive Research (N8 CIR) provided and funded by the N8 research partnership and EPSRC (Grant No. EP/T022167/1). The Centre is co-ordinated by the Universities of Durham, Manchester and York. The authors would also like to thank Martin Walker for providing the code to calculate the chirality order parameters.

Notes and references

1 R. B. Meyer, in *Les Houches Summer School in Theoretical Physics*, ed. R. G. Balian and G. Weil, Gordon and Breach, New York, 1976, pp. 273–373.
2 I. Dozov, *Europhys. Lett.*, 2001, **56**, 247–253.
3 R. Memmer, *Liq. Cryst.*, 2002, **29**, 483–496.
4 M. Cestari, S. Diez-Berart, D. A. Dunmur, A. Ferrarini, M. R. de la Fuente, D. J. B. Jackson, D. O. Lopez, G. R. Luckhurst, M. A. Perez-Jubindo, R. M. Richardson, J. Salud, B. A. Timimi and H. Zimmermann, *Phys. Rev. E: Stat., Nonlinear, Soft Matter Phys.*, 2011, **84**, 031704.
5 C. Meyer, G. R. Luckhurst and I. Dozov, *Phys. Rev. Lett.*, 2013, **111**, 067801.
6 D. Chen, J. H. Porada, J. B. Hooper, A. Klittnick, Y. Shen, M. R. Tuchband, E. Korblova, D. Bedrov, D. M. Walba, M. A. Glaser, J. E. Maclennan and N. A. Clark, *Proc. Natl. Acad. Sci. U. S. A.*, 2013, **110**, 15931–15936.
7 V. Borshch, Y. K. Kim, J. Xiang, M. Gao, A. Jákli, V. P. Panov, J. K. Vij, C. T. Imrie, M. G. Tamba, G. H. Mehl and O. D. Lavrentovich, *Nat. Commun.*, 2013, **4**, 2635.
8 M. Sepelj, A. Lesac, U. Baumeister, S. Diele, H. L. Nguyen and D. W. Bruce, *J. Mater. Chem.*, 2007, **17**, 1154–1165.
9 V. P. Panov, M. Nagaraj, J. K. Vij, Y. P. Panarin, A. Kohlmeier, M. G. Tamba, R. A. Lewis and G. H. Mehl, *Phys. Rev. Lett.*, 2010, **105**, 167801.
10 P. A. Henderson and C. T. Imrie, *Liq. Cryst.*, 2011, **38**, 1407–1414.
11 K. Adlem, M. Čopič, G. R. Luckhurst, A. Mertelj, O. Parri, R. M. Richardson, B. D. Snow, B. A. Timimi, R. P. Tuffin and D. Wilkes, *Phys. Rev. E: Stat., Nonlinear, Soft Matter Phys.*, 2013, **88**, 022503.
12 R. J. Mandle, E. J. Davis, S. A. Lobato, C.-C. A. Vol, S. J. Cowling and J. W. Goodby, *Phys. Chem. Chem. Phys.*, 2014, **16**, 6907–6915.
13 R. J. Mandle, E. J. Davis, C. T. Archbold, S. J. Cowling and J. W. Goodby, *J. Mater. Chem. C*, 2014, **2**, 556–566.
14 R. J. Mandle, E. J. Davis, C. T. Archbold, C.-C. A. Voll, J. L. Andrews, S. J. Cowling and J. W. Goodby, *Chem. – Eur. J.*, 2015, **21**, 8158–8167.
15 E. Gorecka, N. Vaupotic, A. Zep, D. Pociecha, J. Yoshioka, J. Yamamoto and H. Takezoe, *Angew. Chem., Int. Ed.*, 2015, **54**, 10155–10159.
16 D. A. Paterson, M. Gao, Y.-K. Kim, A. Jamali, K. L. Finley, B. Robles-Hernández, S. Diez-Berart, J. Salud, M. R. de la Fuente, B. A. Timimi, H. Zimmermann, C. Greco, A. Ferrarini, J. M. D. Storey, D. O. López, O. D. Lavrentovich, G. R. Luckhurst and C. T. Imrie, *Soft Matter*, 2016, **12**, 6827–6840.
17 D. A. Paterson, J. P. Abberley, W. T. A. Harrison, J. M. D. Storey and C. T. Imrie, *Liq. Cryst.*, 2017, **44**, 127–146.
18 D. Chen, M. Nakata, R. Shao, M. R. Tuchband, M. Shuai, U. Baumeister, W. Weissflog, D. M. Walba, M. A. Glaser, J. E. Maclennan and N. A. Clark, *Phys. Rev. E: Stat., Nonlinear, Soft Matter Phys.*, 2014, **89**, 022506.
19 S. P. Sreenilayam, V. P. Panov, J. K. Vij and G. Shanker, *Liq. Cryst.*, 2017, **44**, 244–253.
20 S. M. Jansze, A. Martínez-Felipe, J. M. D. Storey, A. T. M. Marcelis and C. T. Imrie, *Angew. Chem., Int. Ed.*, 2015, **54**, 643–646.
21 R. Walker, D. Pociecha, J. P. Abberley, A. Martinez-Felipe, D. A. Paterson, E. Forsyth, G. B. Lawrence, P. A. Henderson, J. M. D. Storey, E. Gorecka and C. T. Imrie, *Chem. Commun.*, 2018, **54**, 3383–3386.
22 R. Walker, D. Pociecha, A. Martinez-Felipe, J. M. D. Storey, E. Gorecka and C. T. Imrie, *Crystals*, 2020, **10**, 175.
23 R. Walker, D. Pociecha, M. Salamończyk, J. M. D. Storey, E. Gorecka and C. T. Imrie, *Mater. Adv.*, 2020, **1**, 1622–1630.
24 R. J. Mandle, *Soft Matter*, 2016, **12**, 7883–7901.
25 R. Walker, *Liq. Cryst. Today*, 2020, **29**, 2–14.
26 R. Walker, D. Pociecha, J. M. D. Storey, E. Gorecka and C. T. Imrie, *Chem. – Eur. J.*, 2019, **25**, 13329–13335.
27 J. P. Abberley, R. Killah, R. Walker, J. M. D. Storey, C. T. Imrie, M. Salamończyk, C. Zhu, E. Gorecka and D. Pociecha, *Nat. Commun.*, 2018, **9**, 228.
28 R. Walker, D. Pociecha, G. J. Strachan, J. M. D. Storey, E. Gorecka and C. T. Imrie, *Soft Matter*, 2019, **15**, 3188–3197.
29 M. Salamończyk, N. Vaupoti, D. Pociecha, R. Walker, J. M. D. Storey, C. T. Imrie, C. Wang, C. Zhu and E. Gorecka, *Nat. Commun.*, 2019, **10**, 1922.
30 J. Xiang, Y. Li, Q. Li, D. A. Paterson, J. M. D. Storey, C. T. Imrie and O. D. Lavrentovich, *Adv. Mater.*, 2015, **27**, 3014–3018.
31 J. Xiang, A. Varanytsia, F. Minkowski, D. A. Paterson, J. M. D. Storey, C. T. Imrie, O. D. Lavrentovich and P. Palffy-Muhoray, *Proc. Natl. Acad. Sci. U. S. A.*, 2016, **113**, 12925–12928.
32 M. Mrukiewicz, O. S. Iadlovska, G. Babakhanova, S. Siemianowski, S. V. Shiyanovskii and O. D. Lavrentovich, *Liq. Cryst.*, 2019, **46**, 1544–1550.
33 S. K. Prasad, P. L. Madhuri, P. Satapathy and C. V. Yelamaggad, *Appl. Phys. Lett.*, 2018, **112**, 253701.
34 V. Sridurai, M. B. Kanakala, C. V. Yelamaggad and G. G. Nair, *Soft Matter*, 2019, **15**, 9982–9990.
35 S. Aya, P. Salamon, D. A. Paterson, J. M. D. Storey, C. T. Imrie, F. Araoka, A. Jákli and A. Buka, *Adv. Mater. Interfaces*, 2019, **6**, 1802032.
36 C. Feng, J. Feng, R. Saha, Y. Arakawa, J. Gleeson, S. Sprunt, C. Zhu and A. Jákli, *Phys. Rev. Res.*, 2020, **2**, 032004.
37 C. Zannoni, *Liq. Cryst.*, 2018, **45**, 1880–1893.
38 C. Zannoni, *J. Mater. Chem.*, 2001, **11**, 2637–2646.

39 P. Pasini and C. Zannoni, *Advances in the Computer Simulatons of Liquid Crystals*, Springer, Dordrecht, 1999.
40 M. P. Allen, *Liq. Cryst.*, 2019, **117**, 2391–2417.
41 M. R. Wilson, *Chem. Soc. Rev.*, 2007, **36**, 1881–1888.
42 N. J. Boyd and M. R. Wilson, *Phys. Chem. Chem. Phys.*, 2015, **17**, 24851–24865.
43 M. J. Cook and M. R. Wilson, *J. Chem. Phys.*, 2000, **112**, 1560–1564.
44 M. R. Wilson and D. J. Earl, *J. Mater. Chem.*, 2001, **11**, 2672–2677.
45 M. P. Neal, M. Solymosi, M. R. Wilson and D. J. Earl, *J. Chem. Phys.*, 2003, **119**, 3567–3573.
46 D. J. Earl and M. R. Wilson, *J. Chem. Phys.*, 2003, **119**, 10280–10288.
47 D. J. Earl and M. R. Wilson, *J. Chem. Phys.*, 2004, **120**, 9679–9683.
48 D. J. Earl, M. A. Osipov, H. Takezoe, Y. Takanishi and M. R. Wilson, *Phys. Rev. E: Stat., Nonlinear, Soft Matter Phys.*, 2005, **71**, 021706.
49 J. Peláez and M. R. Wilson, *Phys. Rev. Lett.*, 2006, **97**, 267801.
50 N. J. Boyd and M. R. Wilson, *Phys. Chem. Chem. Phys.*, 2018, **20**, 1485–1496.
51 S.-Y. Jo, B.-C. Kim, S.-W. Jeon, J.-H. Bae, M. Walker, M. Wilson, S.-W. Choi and H. Takezoe, *RSC Adv.*, 2017, **7**, 1932–1935.
52 B.-C. Kim, M. Walker, S.-Y. Jo, M. R. Wilson, H. Takezoe and S.-W. Choi, *RSC Adv.*, 2018, **8**, 1292–1295.
53 J. S. Lintuvuori, G. Yu, M. Walker and M. R. Wilson, *Liq. Cryst.*, 2018, **45**, 1996–2009.
54 S. Shadpour, A. Nemati, N. J. Boyd, L. Li, M. E. Prévôt, S. L. Wakerlin, J. P. Vanegas, M. Salamończyk, E. Hegmann, C. Zhu, M. R. Wilson, A. I. Jákli and T. Hegmann, *Mater. Horiz.*, 2019, **6**, 959–968.
55 S. Shadpour, A. Nemati, M. Salamończyk, M. E. Prévôt, J. Liu, N. J. Boyd, M. R. Wilson, C. Zhu, E. Hegmann, A. I. Jákli and T. Hegmann, *Small*, 2020, **16**, 1905591.
56 M. R. Wilson, *J. Chem. Phys.*, 1998, **107**, 8654–8663.
57 A. G. Vanakaras and D. J. Photinos, *Liq. Cryst.*, 2018, **45**, 2184–2196.
58 C. Greco and A. Ferrarini, *Phys. Rev. Lett.*, 2015, **115**, 147801.
59 M. Chiappini, A. Patti and M. Dijkstra, *Phys. Rev. E*, 2020, **102**, 040601.
60 M. Chiappini and M. Dijkstra, *Nat. Commun.*, 2021, **12**, 2157.
61 M. Chiappini, T. Drwenski, R. van Roij and M. Dijkstra, *Phys. Rev. Lett.*, 2019, **123**, 068001.
62 J. Wang, R. M. Wolf, J. W. Caldwell, P. A. Kollman and D. A. Case, *J. Comput. Chem.*, 2004, **25**, 1157–1174.
63 J. Wang, W. Wang, P. A. Kollman and D. A. Case, *J. Mol. Graphics Modell.*, 2006, **25**, 247–260.
64 A. Jakalian, D. B. Jack and C. I. Bayly, *J. Comput. Chem.*, 2002, **23**, 1623–1641.
65 A. W. S. da Silva and W. F. Vranken, *BMC Res. Notes*, 2012, **5**, 367.
66 S. Pronk, S. Páll, R. Schulz, P. Larsson, P. Bjelkmar, R. Apostolov, M. R. Shirts, J. C. Smith, P. M. Kasson, D. van der Spoell, B. Hess and E. Lindahl, *Bioinformatics*, 2013, **29**, 845–854.
67 U. Essmann, L. Perera, M. L. Berkowitz, T. Darden, H. Lee and L. G. Pedersen, *J. Chem. Phys.*, 1995, **103**, 8577–8593.
68 H. J. C. Berendsen, J. P. M. Postma, W. F. van Gunsteren, A. DiNola and J. R. Haak, *J. Chem. Phys.*, 1984, **81**, 3684–3690.
69 S. Nosé, *J. Chem. Phys.*, 1984, **81**, 511–519.
70 W. G. Hoover, *Phys. Rev. A: At., Mol., Opt. Phys.*, 1985, **31**, 1695–1697.
71 M. Parrinello and A. Rahman, *J. Appl. Phys.*, 1981, **52**, 7182–7190.
72 B. Hess, H. Bekker, H. J. C. Berendsen and J. G. E. M. Fraaije, *J. Comput. Chem.*, 1997, **18**, 1463–1472.
73 W. Humphrey, A. Dalke and K. Schulten, *J. Mol. Graphics*, 1996, **14**, 33–38.
74 A. Ferrarini, G. J. Moro and P. L. Nordio, *Liq. Cryst.*, 1995, **19**, 397–399.
75 A. Ferrarini, G. J. Moro and P. L. Nordio, *Mol. Phys.*, 1996, **87**, 485–499.
76 A. Ferrarini, G. Gottarelli, P. L. Nordio and G. P. Spada, *J. Chem. Soc., Perkin Trans. 2*, 1999, 411–418.
77 A. di Matteo, S. M. Todd, G. Gottarelli, G. Solladie, V. E. Williams, R. P. Lemieux, A. Ferrarini and G. P. Spada, *J. Am. Chem. Soc.*, 2001, **123**, 7842–7851.
78 Y. Vorobjev and J. Hermans, *Biophys. J.*, 1997, **73**, 722–732.
79 A. J. Stone, *Mol. Phys.*, 1978, **36**, 241–256.
80 C. Meyer, G. R. Luckhurst and I. Dozov, *J. Mater. Chem. C*, 2015, **3**, 318–328.
81 G. Singh, J. Fu, D. M. Agra-Kooijman, J.-K. Song, M. R. Vengatesan, M. Srinivasarao, M. R. Fisch and S. Kumar, *Phys. Rev. E*, 2016, **94**, 060701.
82 R. J. Mandle and J. W. Goodby, *Phys. Chem. Chem. Phys.*, 2019, **21**, 6839–6843.
83 G. Yu, M. Walker and M. R. Wilson, *Phys. Chem. Chem. Phys.*, 2021, **23**, 6408–6421.
84 J. W. Emsley, M. Lelli, A. Lesage and G. R. Luckhurst, *J. Phys. Chem. B*, 2013, **117**, 6547–6557.
85 C. Zhang, N. Diorio, O. D. Lavrentovich and A. Jákli, *Nat. Commun.*, 2014, **5**, 3302.
86 A. Varanytsia and L.-C. Chien, *J. Appl. Phys.*, 2016, **119**, 014502.
87 Y.-C. Lin, P.-C. Wu and W. Lee, *Photonics Res.*, 2019, **7**, 1258–1265.
88 C. T. Imrie and P. A. Henderson, *Chem. Soc. Rev.*, 2007, **36**, 2096–2124.
89 A. Ferrarini, G. R. Luckhurst, P. L. Nordio and S. J. Roskilly, *J. Chem. Phys.*, 1994, **100**, 1460–1469.
90 G. R. Luckhurst and S. Romano, *J. Chem. Phys.*, 1997, **107**, 2557–2572.
91 C. Greco, G. R. Luckhurst and A. Ferrarini, *Soft Matter*, 2014, **10**, 9318–9323.
92 E. Cruickshank, M. Salamończyk, D. Pociecha, G. J. Strachan, J. M. D. Storey, C. Wang, J. Feng, C. Zhu, E. Gorecka and C. T. Imrie, *Liq. Cryst.*, 2019, **46**, 1595–1609.
93 E. E. Pocock, R. J. Mandle and J. W. Goodby, *Soft Matter*, 2018, **14**, 2508–2514.
94 M. R. Wilson and M. P. Allen, *Liq. Cryst.*, 1992, **12**, 157–176.
95 M. R. Wilson, *Liq. Cryst.*, 1996, **21**, 437–447.

96 C. Greco, G. R. Luckhurst and A. Ferrarini, *Phys. Chem. Chem. Phys.*, 2013, **15**, 14961–14965.
97 Y. Arakawa, K. Komatsu and H. Tsuji, *New J. Chem.*, 2019, **43**, 6786–6793.
98 Y. Arakawa, K. Komatsu, S. Inui and H. Tsuji, *J. Mol. Struct.*, 2020, **1199**, 126913.
99 Y. Arakawa, K. Komatsu, T. Shiba and H. Tsuji, *Mater. Adv.*, 2021, **2**, 1760–1773.
100 D. A. Paterson, J. P. Abberley, W. T. A. Harrison, J. M. D. Storey and C. T. Imrie, *Liq. Cryst.*, 2017, **44**, 127–146.
101 Y. Arakawa, K. Komatsu, T. Shiba and H. Tsuji, *J. Mol. Liq.*, 2021, **326**, 115319.
102 T. D. Potter, M. Walker and M. R. Wilson, *Soft Matter*, 2020, **16**, 9488–9498.
103 G. Yu and M. R. Wilson, *J. Mol. Liq.*, 2022, **345**, 118210.